RSC Advances

ROYAL SOCIETY OF CHEMISTRY

www.rsc.org/advances

Formation of orthorhombic SnO_2 originated from lattice distortion by Mn-doped tetragonal SnO_2

Qian Zhang,[a] Peng Liu,[b] Chunjie Miao,[a] Zhiwen Chen,[*,a,b] C. M. Lawrence Wu,[b] Chan-Hung Shek[*,b]

[a] Shanghai Applied Radiation Institute, School of Environmental and Chemical Engineering, Shanghai University, Shanghai 200444, People's Republic of China

[b] Department of Physics and Materials Science, City University of Hong Kong, Tat Chee Avenue, Kowloon Tong, Hong Kong

[*]Corresponding authors. Tel.: +86 21 66137503. Fax: +86 21 66137787. E-mail: zwchen@shu.edu.cn; apchshek@cityu.edu.hk.

[a] Shanghai Applied Radiation Institute, School of Environmental and Chemical Engineering, Shanghai University, Shanghai 200444, People's Republic of China

[b] Department of Physics and Materials Science, City University of Hong Kong, Tat Chee Avenue, Kowloon Tong, Hong Kong

Abstract

Tin dioxide (SnO_2) is an *n*-type semiconductor material with tetragonal rutile crystal structure under normal conditions and displays many interesting physical and chemical properties. Another form of SnO_2 with an orthorhombic crystal structure is known to be stable only at high pressures and temperatures. However, there are limited reports on effects of Mn-doped tetragonal phase SnO_2 on micro/nanostructured characteristics. In this article, micro/nanostructures of Mn-doped tetragonal phase SnO_2 have been successfully prepared by chemical co-precipitation method. The micro/nanostructural evolution of Mn-doped tetragonal phase SnO_2 under different heat treatment temperatures is evaluated by X-ray diffraction (XRD) and high-resolution transmission electron microscopy. It is surprisingly found that the orthorhombic phase SnO_2 is formed in Mn-doped tetragonal phase SnO_2. The obvious diffraction peaks and clear lattice fringes confirmed that the orthorhombic phase SnO_2 nanocrystals evidently exist in Mn-doped SnO_2 samples. Experimental results indicated that the XRD peak intensities and crystal planes of the orthorhombic phase SnO_2 decrease with increasing of heat treatment temperatures. Formation of orthorhombic phase SnO_2 is attributed to the lattice distortion of tetragonal phase SnO_2 due to the Mn-doped tetragonal phase SnO_2.

Keywords: Tin dioxide; Tetragonal; Orthorhombic; Lattice distortion; Micro/nanostructure

Introduction

Tin dioxide (SnO_2) is a unique material of widespread technological applications, particularly in the field of strategic functional materials. SnO_2, as a kind of *n*-type wide-band-gap semiconductor material (E_g = 3.64 eV at 300 K), has been extensively and intensively studied in the past few years,[1-4] which exhibited superior properties such as transparency, remarkable chemical and thermal stabilities, used in solar cells,[5,6] gas sensors,[7,8] electrode materials,[9,10] catalysts,[11] and optoelectronic devices.[12,13] It has been noted that the most important form of SnO_2 is cassiterite, a phase of SnO_2 with the tetragonal rutile crystal structure. In recent years, the micro/nanostructural characteristics and prosperities of tetragonal phase SnO_2 have been extensively studied by our and other research groups,[14-17] motivated in part by many technological applications in gas sensing, optical and electrical properties.[18-22]

In addition to the stable tetragonal phase SnO_2, it existed another form and was called orthorhombic phase crystal structure (a = 0.4714 nm, b = 0.5727 nm, and c = 0.5214 nm).[14] However, orthorhombic phase SnO_2 has been seldom investigated in the past few years because it is metastable structure. It is known that the orthorhombic phase SnO_2 was usually found in high pressure and temperature experiments. For example, Suito's research group has first synthesized SnO_2 powders with an orthorhombic phase structure at a high pressure of 15.8 GPa and a temperature of 800 °C.[23] The orthorhombic phase SnO_2 has also been formed in diamond-anvil SnO_2 experiments by Liu,[24] who found that it was formed from a higher-pressure fluorite-type phase upon release of pressure. Joseph Lai and Shek's research group detected the orthorhombic phase in X-ray scattering measurements of SnO_2 powders.[25] Ultrafine oxidized tin particles with particle size about 6 nm have been prepared by inert gas condensation deposition under low oxygen pressure. They believed that the orthorhombic phase SnO_2 may be an intermediate product when disordered tin

oxide (amorphous or nanoparticle) transforms to stable tin oxide (rutile phase) on annealing under oxygen deficiency conditions. Kaplan also reported that both tetragonal and orthorhombic SnO_2 phases were found in Sn-O films deposited at substrate temperatures in the range 350-500°C.[26] The high-pressure orthorhombic phase SnO_2 is believed to have the same crystal structure as α-PbO_2, which was refined by Kong et al. using a high vacuum metal organic chemical vapor deposition (MOCVD) system.[27] A similar sequence of orthorhombic phase SnO_2 was reported by our research group in studies of SnO_2 thin films using pulsed laser deposition (PLD).[28,29] Above experimental results indicated that the orthorhombic phase SnO_2 can be synthesized by a variety of technological routes. It can be reasonable to extrapolate that the high pressures/temperatures or strain may be the vital factors for the formation of the orthorhombic phase SnO_2.

Transition metal Mn-doped tetragonal SnO_2 may induce their lattice distortion since the Mn^{3+} (0.65 Å) or Mn^{4+} (0.54 Å) ionic radius is smaller than that of Sn^{4+} (0.69 Å),[30] which will result in high compressive stresses or high pressures on the SnO_2 and generate the orthorhombic phase SnO_2. However, this strategy has not been reported so far. Sangaletti and co-workers have reported SnO_2 multilayer thin film grown by the rheotaxial growth and thermal oxidation method on Al_2O_3 substrates.[31] Their results indicated that, in addition to the SnO_2 cassiterite phase, a contribution from another SnO_2 orthorhombic phase was present, which can be related to cassiterite by introducing micro-twinning effects. This SnO_2 multilayer thin film showed a higher sensitivity towards CO with respect to the conventional single layer SnO_2 sensors. The formation of orthorhombic-phase SnO_2 is intimately tied to a number of important synthesis parameters such as high pressures and temperatures.[23,24,32] Müller found an unknown epitaxial interface phase of SnO_2 on α-quartz $(10\bar{1}0)$, which indicated that different octahedra stacking in the case of SnO_2 may give rise to different orthorhombic possibilities.[33] Arbiol and co-workers have reported the synthesis of

pure monocrystalline orthorhombic SnO_2 nanowires and pure monocrystalline orthorhombic SnO_2 nanowires decorated with cassiterite SnO_2 nanoclusters.[34] In fact, when previous experiments are examined in detail, it is often difficult to rule out the possibility of the presence of high compressive stress.

In this article, the doping of tetragonal phase SnO_2 particles with Mn ions will be carried out using a simple chemical co-precipitation method. The micro/nanostructures of Mn-doped tetragonal phase SnO_2 under different heat treatment temperatures are evaluated in detail by X-ray diffraction (XRD) and high-resolution transmission electron microscopy (HRTEM). We corroborated the coexistence of both tetragonal and orthorhombic SnO_2 phases in Mn-doped SnO_2 samples under different heat treatment temperatures. The obvious XRD peaks and clear lattice fringes observed by HRTEM confirmed that the orthorhombic phase SnO_2 nanocrystals evidently exist in Mn-doped SnO_2 samples. Experimental results indicated that the XRD peak intensities and crystal planes of the orthorhombic phase SnO_2 decrease with increasing of heat treatment temperatures. The micro/nanostructural analyses certificated that the crystallographic structure and lattice mismatch at the interface between tetragonal and orthorhombic SnO_2 phases is very important in defining the micro/nanostructure characteristics. The strain originated by the different lattice parameters of the tetragonal and orthorhombic SnO_2 in relation to the doping of tetragonal phase SnO_2 particles with Mn ions may play a critical role in formation of the orthorhombic phase SnO_2.

Experimental

All chemicals used in this experiment were analytical grade without further purification. A typical procedure to synthesize Mn-doped SnO_2 particles was performed as follows: the Mn-doped tetragonal phase SnO_2 particles were prepared by a simple chemical co-precipitation method using

$SnCl_2 \cdot 2H_2O$ and $MnCl_2 \cdot 6H_2O$ as the sources of Sn and Mn ions. The $SnCl_2 \cdot 2H_2O$ was added in de-ionized water (0.2 mol/L) and mixed with $MnCl_2 \cdot 6H_2O$ (5 mol%) homogeneously. The above mixed solution was refluxed at 130 ^oC for 36 h under air atmosphere. The precipitation was carried out using aqueous ammonia (1 mol/L) after cooling the refluxed solution. The primal sample was washed several times with de-ionized water to remove the water-soluble impurities and free reactants and dried at 80 ^oC for 10 h. In order to obtain the better crystalline SnO_2 particles, the as-precursor was calcined in air at four different temperatures: 250, 350, 450, and 550 °C for 3 h, respectively. In order to better understand the effects of the Mn-doped SnO_2 particles, a pure tetragonal phase SnO_2 sample was also prepared using a similar method and calcined in the same conditions. The micro/nanostructural evolution of the resultant powders was characterized by X-ray diffraction (XRD) and high-resolution transmission electron microscopy (HRTEM) techniques.

XRD patterns were obtained from Japan Regaku D/max-2500 using Cu K_α radiation in reflection geometry. A proportional counter with an operating voltage of 40 kV and a current of 40 mA was used. XRD patterns were recorded at a scanning rate of $0.08^o s^{-1}$ in the 2θ ranges from 20 to 60^o. HRTEM observations were performed on a JEOL JEM-2010F transmission electron microscope operating at 200 kV.

Results and discussion

The crystalline evolution of samples from the as-synthesized powders during heat treatment in air for different temperatures was investigated by XRD techniques. Fig. 1 shows the typical XRD patterns of the undoped samples which were taken from the as-synthesized sample (Fig. 1A) and heat treatment in air for 250 °C (Fig. 1B), 350 °C (Fig. 1C), 450 °C (Fig. 1D), and 550 °C (Fig. 1E). The XRD patterns at various heat treatment temperatures show that the peak intensities and sharpnesses

are enhanced with compared to the as-synthesized sample, indicating the undoped samples at various heat treatment temperatures are well-crystallized. The presence of the broad and weak peaks as shown in Fig. 1A indicated that the nanoparticles of the as-synthesized sample are smaller than heat treatment one because the width of the XRD peaks is related to the particle size through Scherrer's formula: $D = K\lambda/\beta\cos\theta$, where D is the diameter of the nanoparticles, $K = 0.9$, λ (Cu Kα) = 1.5406 Å, and β is the full width at half-maximum of the diffraction peak. The major diffraction peaks of all undoped samples corresponded to the tetragonal unit cell structure of SnO_2 with lattice constants $a = b = 4.738$ Å and $c = 3.187$ Å, which are consistent with the standard values for bulk SnO_2 (International Center for Diffraction Data, PDF File No. 41-1445). The observed (*hkl*) peaks are (110), (101), (200), (211), (220), and (002). Comparing with Fig. 1A and Fig. 1B-E, it can be confirmed that the growth of the SnO_2 nanoparticles is influenced significantly by heat treatment temperatures. Experimental results indicated that the grain size of the undoped SnO_2 nanoparticles increases with increasing of heat treatment temperatures. All peaks as shown in Fig. 1B-E became sharp and stronger, proving that the heat treatment temperature is a potentially powerful technique to improve the growth of SnO_2 nanocrystals. However, it is not able to find the surprise changes in the undoped SnO_2 samples. We will investigate in detail the effects of Mn-doping of tetragonal phase SnO_2 on micro/nanostructural characteristics.

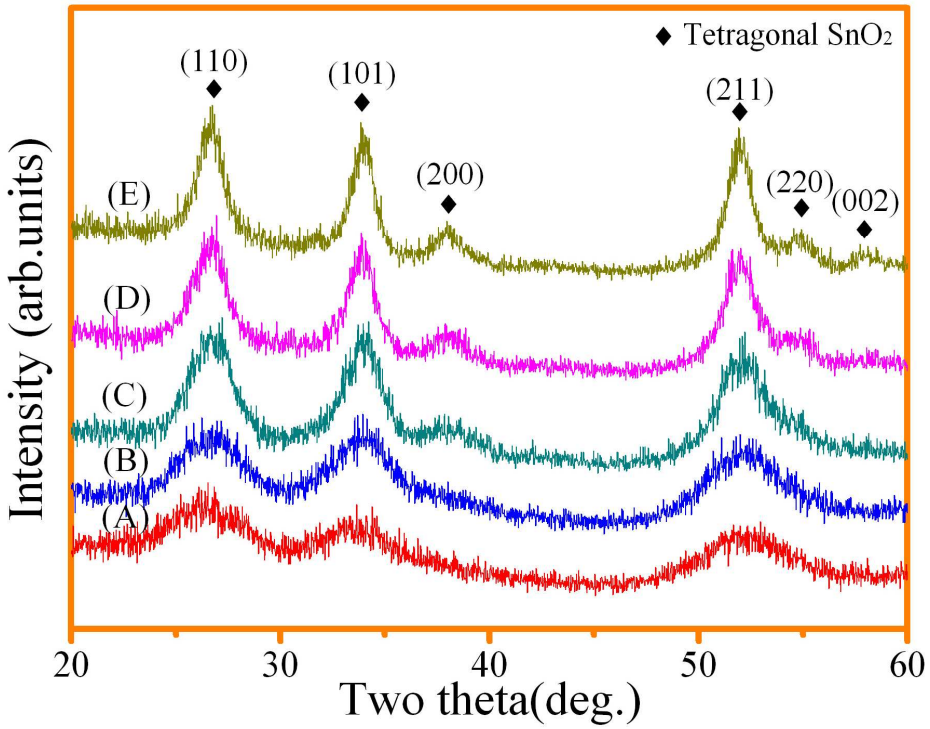

Fig. 1 The typical XRD patterns of pure tetragonal phase SnO_2 nanoparticles after heat treatment in air for (A) as-synthesized, (B) 250 °C, (C) 350 °C, (D) 450 °C, and (E) 550 °C.

In order to search of novel micro/nanostructured materials with orthorhombic features along with precise controllable physical and chemical properties, the wide band gap oxides such as SnO_2, TiO_2, ZnO, and HfO_2 doped with transition metal ions such as Mn, Co, Ni, Fe, Cr, etc. have attracted considerable attention due to a number of distinctive optical and electronic properties originating from large *sp-d* exchange interaction between the transition metal ions and the band electrons.[35] Fig. 2 represents the typical XRD patterns of the Mn-doped tetragonal phase SnO_2 with the Mn = 5 mol% which were taken from the as-synthesized sample (Fig. 2A) and heat treatment in air for 250 °C (Fig. 2B), 350 °C (Fig. 2C), 450 °C (Fig. 2D), and 550 °C (Fig. 2E). It was surprised to find that the Mn-doped samples of the as-synthesized and heat treatment at various temperatures were composed of orthorhombic and tetragonal SnO_2. The diffraction peaks at (110), (101), (200), (211), (220), and (002) planes can be indexed to the tetragonal phase SnO_2 and the reflections at (110), (111), (021),

(022), (130), and (113) planes are attributed to the orthorhombic unit cell of SnO_2. The higher heat treatment temperature gave rise to an increase in the peak intensity of tetragonal phase SnO_2 at the expense of orthorhombic phase SnO_2. However, the Mn-doped sample heated even up to 550 ^oC was still composed of a mixture of orthorhombic and tetragonal SnO_2. The experimental results indicated that there were no extra peaks of manganese oxides such as MnO, Mn_2O_3, MnO_2, Mn_3O_4, and any Sn/Mn ternary oxides, implying that the transition metal ions have substituted at the Sn^{4+} sites. Furthermore, the peak position shifted to larger angle at the Mn-doped samples, revealing possible changes in lattice parameters. As the heat-treatment temperature increasing, the peaks of the Mn-doped samples have no obvious changes, suggesting that a portion of the metal oxide ions formed stable solid solutions with SnO_2 and occupied in the regular lattice sites of SnO_2.

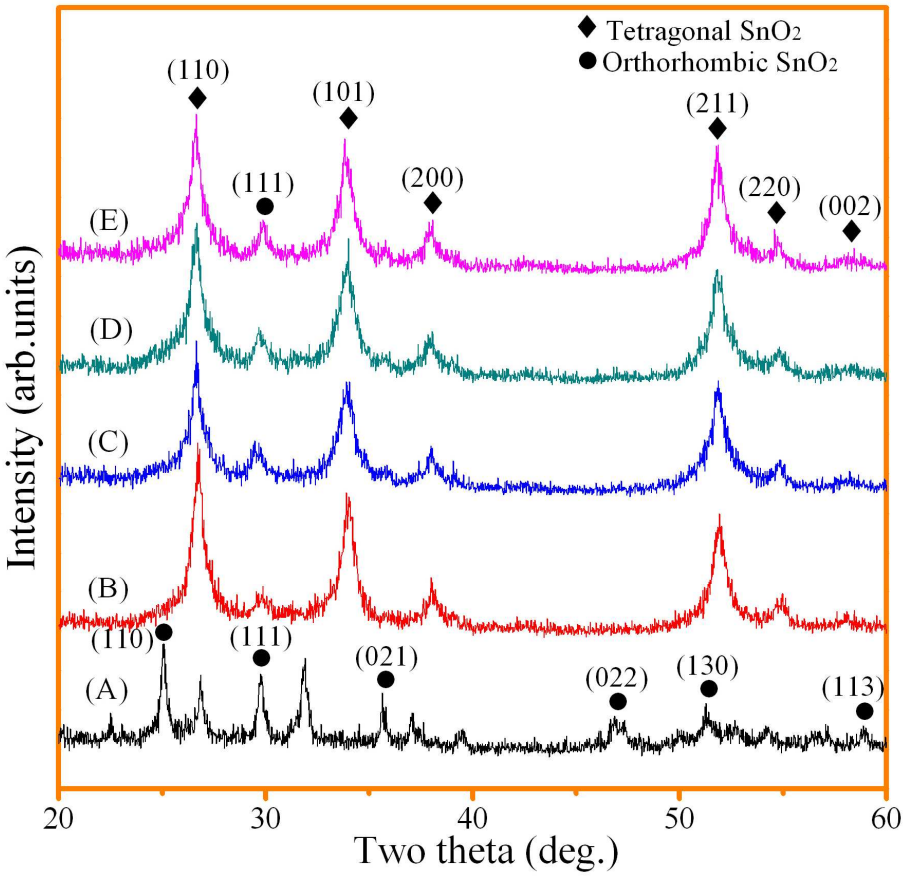

Fig. 2 The typical XRD patterns of Mn-doped tetragonal phase SnO_2 (Mn = 5 mol%) after heat treatment in air for (A) as-synthesized, (B) 250 °C, (C) 350 °C, (D) 450 °C, and (E) 550 °C.

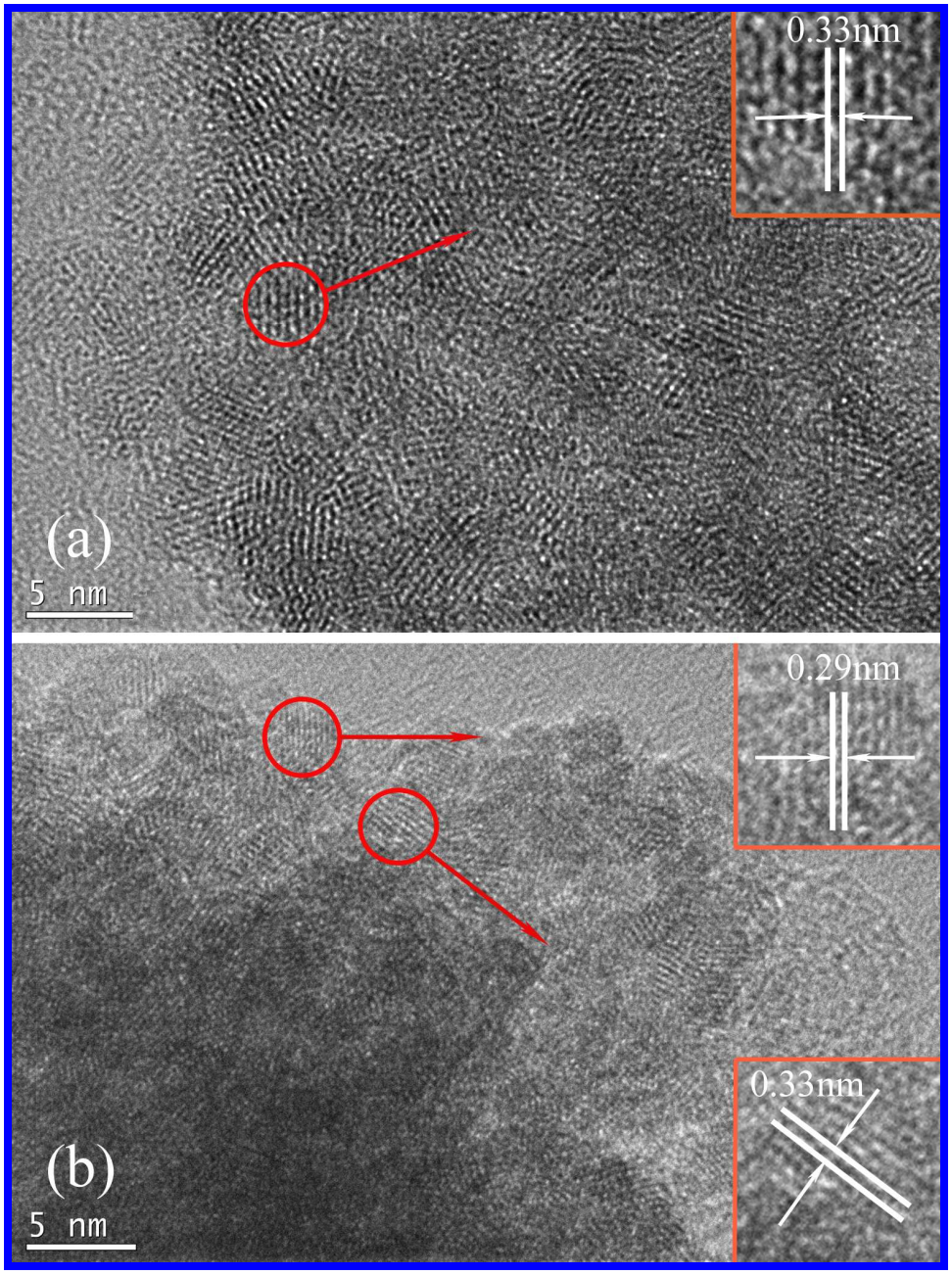

Fig. 3 The typical HRTEM micrographs of (a) as-synthesized undoped SnO_2 nanoparticles and (b) as-synthesized Mn-doped SnO_2 (Mn = 5 mol%).

In order to understand the precise formation processes of the orthorhombic phase SnO_2 and their relation to micro/nanostructure with tetragonal phase SnO_2 by the Mn-doping, we will investigate the possible mechanism to explain the crystallographic behavior. HRTEM observations in relation to

the Mn-doping of tetragonal phase SnO_2 particles at different heat treatment temperatures can give useful information about local composition and lattice mismatch at dislocation cores. A more detailed analysis can be made based on the highly magnified HRTEM images as shown in Fig. 3, which were taken from the as-synthesized undoped SnO_2 nanoparticles as shown in Fig. 3a and as-synthesized Mn-doped SnO_2 (Mn = 5 mol%) as shown in Fig. 3b. It can be found that the vague lattice fringes were formed in the as-synthesized undoped and Mn-doped samples. It appeared that the surface layer of the as-synthesized undoped and Mn-doped samples is covered with the amorphous oxides since a long-range ordering of lattice planes is not observed. However, the detailed crystallographic analysis indicated that some of the observed lattice fringes may originate from different crystal structure. The lattice fringes observed in Fig. 3a demonstrated that the as-synthesized undoped sample is composed of ultrafine nanoparticles with a diameter below 5 nm, even if it is greater than one of Fig. 3b. On closer inspection, the recurrent values of separation distance between lattice layers are found (in particular, 0.33 nm), which corresponds to the lattice parameters of the tetragonal structure of SnO_2 (evidenced in the inset of Fig. 3a). Simultaneously, it is found from the as-synthesized Mn-doped sample (Fig. 3b) that, besides the tetragonal phase SnO_2 related to the crystal plane (110), the (111) crystal plane also was observed, which corresponds to the interplanar spacing (0.29 nm) of the orthorhombic phase SnO_2 as shown in the inset of Fig. 3b. The average nanoparticle size was less than 3 nm. A more detailed analysis from Fig. 3b indicated that the slight misorientations are visible in the HRTEM image of a nanocluster composed of several primary SnO_2 nanocrystallines. These misorientations or defects originated from imperfect attachment among several nanocrystallines, resulting in the edge and screw dislocations. The strain originated by the different lattice parameters of the tetragonal and orthorhombic SnO_2 in relation to the Mn-doping of tetragonal SnO_2 particles may play a critical role in formation of the orthorhombic

phase SnO_2. Above experimental results indicated that both tetragonal and orthorhombic SnO_2 phases are coexisted in the as-synthesized Mn-doped SnO_2 sample, which is consistent with the XRD results as shown in Fig. 2A.

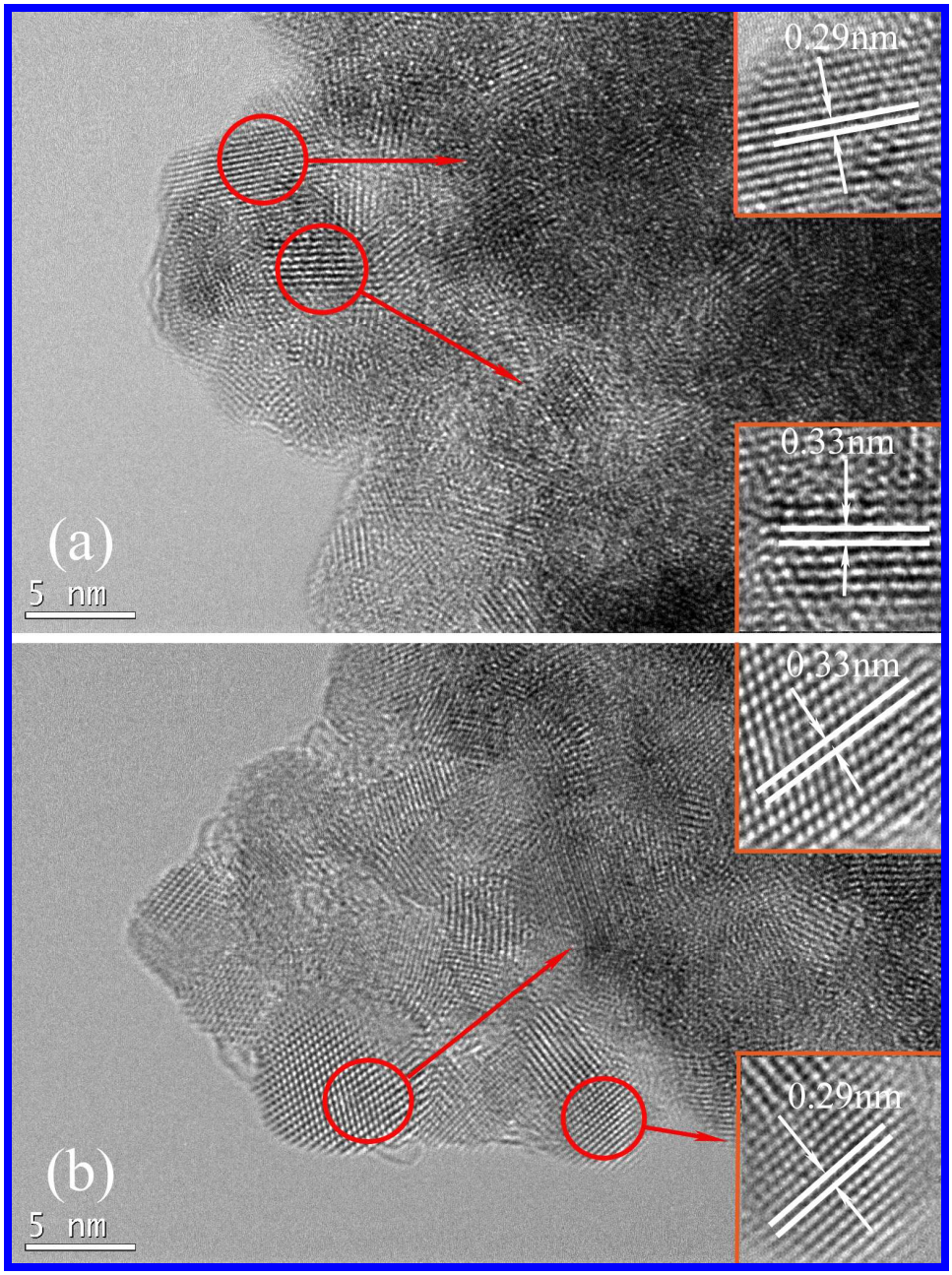

Fig. 4 The typical HRTEM micrographs of Mn-doped SnO_2 (Mn = 5 mol%) after being heated at (a) 250 °C and (b) 350 °C.

It is known that the SnO_2 with an orthorhombic structure was stable only at high pressures and

temperatures, and was a metastable phase under normal conditions. Further advancement of the formation processes for this orthorhombic phase SnO_2 requires a clear understanding of its thermal stabilities. Fig. 4 shows the typical HRTEM micrographs of the Mn-doped SnO_2 (Mn = 5 mol%) after being heated at (a) 250 °C (Fig. 4a) and (b) 350 °C (Fig. 4b). It can be seen that the crystallinity properties of the Mn-doped SnO_2 heated at 250 °C and 350 °C increased with increasing of the heat treatment temperatures, comparing to the as-synthesized Mn-doped SnO_2 as shown in Fig. 3b. Many long-range ordered lattice fringes can be clearly observed in the Mn-doped SnO_2 and the average nanoparticle sizes increased with increasing of the heat treatment temperatures as shown in Fig. 4. When the Mn-doped SnO_2 sample heated to 250 °C, the (110) crystal plane related to the tetragonal SnO_2 and (111) crystal plane connected with the orthorhombic SnO_2 were clearly observed. Moreover, the average nanoparticle size increased to about 5 nm as shown in Fig. 4a. When the Mn-doped SnO_2 sample heated to 350 °C, the lattice firings became much clearer, and the average nanoparticle size increased to about 7 nm as shown in Fig. 4b. The experimental results indicated that the heat-treatment effects could improve the growth of the SnO_2 nanoparticles.

When the Mn-doped SnO_2 (Mn = 5 mol%) samples were heated up to higher temperatures, e.g. 450 °C and 550 °C, the careful XRD examinations revealed that the Mn-doped SnO_2 samples displayed the coexistence of the tetragonal and orthorhombic SnO_2 as shown in Fig. 2D and E, respectively. In order to examine the micro/nanostructure evolution of the Mn-doped SnO_2 (Mn = 5 mol%) samples at the higher heat-treatment temperatures, further HRTEM investigations are presented in Fig. 5, which shows the typical HRTEM micrographs of the Mn-doped SnO_2 (Mn = 5 mol%) after being heated at (a) 450 °C (Fig. 5a) and (b) 550 °C (Fig. 5b). It can be seen that both SnO_2 phases, tetragonal and orthorhombic structures, were still randomly distributed in the higher temperature heat treatment samples. The gradual growth of the tetragonal SnO_2 at the expense of the

orthorhombic SnO_2 was observed in the micro/nanostructure evolution. The (110) crystal plane related to the tetragonal SnO_2 and (111) crystal plane connected with the orthorhombic SnO_2 can be more clearly observed in the insets of Fig. 5a and b. The misorientations and defects reduced and the lattice fringes were more perfect with increasing of the heat treatment temperatures. The average nanoparticle size increased to about 8 nm and 10 nm as shown in Fig. 5a and b, respectively. All the above experimental results proved that the strain originated by the different lattice parameters of the tetragonal and orthorhombic SnO_2 in relation to the Mn-doping of the tetragonal phase SnO_2 may play a critical role in formation of the orthorhombic phase SnO_2.

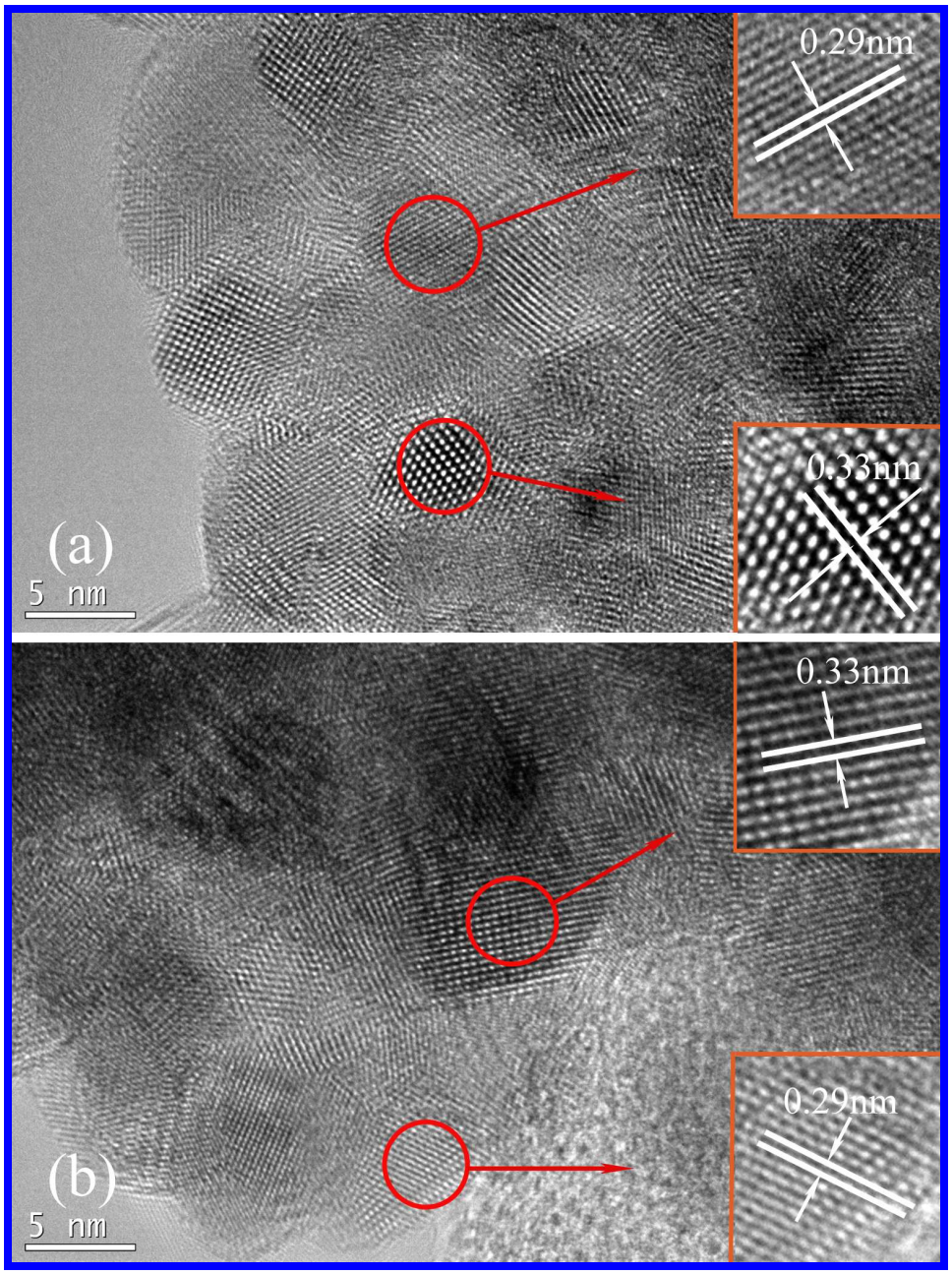

Fig. 5 The typical HRTEM micrographs of Mn-doped SnO_2 (Mn = 5 mol%) after being heated at (a) 450 °C and (b) 550 °C.

A detailed process of the transformation mechanism must take into account the instability of the Mn-doped SnO_2 samples in the temperature range in which the orthorhombic SnO_2 phase begins to form. For the as-synthesized Mn-doped SnO_2 (Mn = 5 mol%) sample, the nonstoichiometric oxides underwent a disproportionation reaction forming tetragonal SnO_2 and perhaps intermediate oxides. If

the intermediate oxides serve as the matrix in which the orthorhombic SnO_2 phase nucleates, then the nucleation must obviously occur before the disproportionation reaction takes place. The formation of the orthorhombic phase SnO_2 is favored by a nucleation barrier which is lower than that for the tetragonal phase SnO_2. The enhancement of the metastable phase could be steric, that is, the formation of the orthorhombic phase SnO_2 may require less atomic rearrangement than the formation of the tetragonal phase SnO_2. As shown by Fig. 2A, the Mn-ions are inclined to incorporate into the tetragonal phase SnO_2 lattice in the form of Mn^{3+} (0.65 Å) or Mn^{4+} (0.54 Å) since their ionic radius is smaller than that of Sn^{4+} (0.69 Å),[30] which led to the shrinkage of the lattice constant due to smaller ionic radius of Mn^{3+} or Mn^{4+} substituted in place of Sn^{4+} sites. When the Mn-ions replaced the Sn^{4+}, the production of the orthorhombic phase SnO_2 increased since the grain size was reduced, perhaps, the reduced grain size inhibited the disproportionation reaction. Such an effect has also been previously detected in a high-temperature X-ray scattering experiment of tin oxide powders with varying particle sizes.[36] In this way, it is therefore appeared more crystal planes of the orthorhombic phase SnO_2 in the as-synthesized Mn-doped sample. On the other hand, the XRD results as shown in Fig. 2B-E indicated that the initial heat treatment sample began to transform into the tetragonal SnO_2 after being heated at 250 °C, 350 °C, 450 °C, and 550 °C, respectively. It was again clearly revealed by the HRTEM observations as shown in Fig. 4 and 5. This research indicated that the strain originated by the different lattice parameters of the tetragonal and orthorhombic SnO_2 in relation to the Mn-doping of the tetragonal phase SnO_2 may play a critical role in formation of the orthorhombic phase SnO_2. The formation of the orthorhombic phase SnO_2 could be attributed to the lattice distortion of the tetragonal phase SnO_2 due to the Mn-doping.

Conclusions

In summary, the micro/nanostructures of the Mn-doped tetragonal phase SnO_2 have been successfully prepared by a chemical co-precipitation method. Their micro/nanostructural evolution under different heat treatment temperatures could be reasonably evaluated by the XRD and HRTEM techniques. It was surprisingly found that the orthorhombic phase SnO_2 could be formed in the Mn-doped tetragonal phase SnO_2. The obvious diffraction peaks and clear lattice fringes confirmed that the orthorhombic phase SnO_2 nanocrystals evidently exist in the Mn-doped SnO_2 samples. Experimental results indicated that the XRD peak intensities and crystal planes of the orthorhombic phase SnO_2 decrease with increasing of the heat treatment temperatures. The formation of orthorhombic phase SnO_2 could be therefore attributed to the lattice distortion of the tetragonal phase SnO_2 due to the Mn-doping. Our findings may enable this novel functional material with the orthorhombic phase SnO_2 to be tailor-made for a large number of applications such as optoelectronic devices and gas sensors.

Acknowledgements

The work described in this article was financially supported by the National Natural Science Foundation of China (Project Numbers: 11375111, 11428410, and 11074161), the Research Fund for the Doctoral Program of Higher Education of China (Project Number: 20133108110021), the Key Innovation Fund of Shanghai Municipal Education Commission (Project Numbers: 14ZZ098 and 10ZZ64), the Science and Technology Commission of Shanghai Municipality (Project Numbers: 14JC1402000 and 10JC1405400), the Shanghai Pujiang Program (Project Number: 10PJ1404100), and the Program for Changjiang Scholars and Innovative Research Team in University (Project

Number: IRT13078). This work was also supported by a grant from the Research Grants Council of the Hong Kong Special Administrative Region, China [Project No. (RGC Ref. No.), CityU 119212].

Notes and references

(1) F. J. Yusta, M. L. Hitchman and S. H. Shamlian, *J. Mater. Chem.,*1997, **7**, 1421-1427.

(2) J. Wang, J. Du, C. Chen, Z. Li, Z. Jiao, M. H. Wu, C. H. Shek, C. M. L. Wu, J. K. L. Lai and Z. W. Chen, *J. Phys. Chem. C*, 2011, **115**, 20523-20528.

(3) H. Huang, C. K. Lim, M. S. Tse, J. Guo and O. K. Tan, *Nanoscale,* 2012, **4**, 1491-1496.

(4) Z. W. Chen, J. K. L. Lai and C. H. Shek, *J. Solid State Chem.*, 2005, **178**, 892-896.

(5) M. A. Hossain, J. R. Jennings, Z. Y. Koh and Q. Wang, *ACS Nano,* 2011, **5**, 3172-3181.

(6) S. Chappel, S. G. Chen and A. Zaban, *Langmuir,* 2002, **18**, 3336-3342.

(7) L. Renard, O. Babot, H. Saadaoui, H. Fuess, J. Broetz, A. Gurlo, E. Arveux, A. Klein and T. Toupance, *Nanoscale*, 2012, **4**, 6806-6813.

(8) A. Kolmakov, D. O. Klenov, Y. Lilach, S. Stemmer and M. Moskovits, *Nano Lett.,* 2005, **5**, 667-673.

(9) Z. F. Du, X. M. Yin, M. Zhang, Q. Y. Hao, Y. G. Wang and T. H. Wang, *Mater. Lett.,* 2010, **64**, 2076-2079.

(10) X. Y. Wang, X. F. Zhou, K. Yao, J.G. Zhang and Z.P. Liu, *Carbon,* 2011, **49**, 133-139.

(11) A. Dodd, A. McKinley, M. Saunders and T. Tsuzuki, *Nanotechnology,* 2006, **1**7, 692-698.

(12) J. S. Lee, S. K. Sim, B. Min, K. Cho, S. W. Kim and S. Kim, *J. Cryst. Growth,* 2004, **267**, 145-149.

(13) H. S. Woo, I. S. Hwang, C. W. Na, S. J. Kim, J. K. Choi, J. S. Lee, J. Choi, G. T. Kim and J. H. Lee, *Mater. Lett.,* 2012, **68**, 60-63.

(14) Z. W. Chen, D. Y. Pan, B. Zhao, G. J. Ding, Z. Jiao, M. H. Wu, C. H. Shek, L. C. M. Wu and J. K. L. Lai, *ACS Nano,* 2010, **4**, 1202-1208.

(15) Z. W. Chen, C. M. L. Wu, C. H. Shek, J. K. L. Lai, Z. Jiao and M. H. Wu, *Crit. Rev. Solid State,* 2008, **33**, 197-209.

(16) L.S. Zhang, L. Y. Jiang, H. J. Yan, W. D. Wang, W. Wang, W. G. Song, Y. G. Guo and L. J. Wan, *J. Mater. Chem.,* 2010, **20**, 5462-5467.

(17) Z. W. Chen, J. K. L. Lai, C. H. Shek and H. D. Chen, *Appl. Phys. A,* 2005, **81**, 959-962.

(18) Y. Wang, H. C. Zeng and J. Y. Lee, *Adv. Mater.*, 2006, **18**, 645-649.

(19) Z.W. Chen, J. K. L. Lai and C. H. Shek, *Phy. Rev. B,* 2004, **70**, 165314-165320.

(20) Z.W. Chen, J. K. L. Lai and C. H. Shek, *Phys. Lett. A*, 2005, **345**, 218-223.

(21) H. T. Ng, J. Li, M. K. Smith, P. Nguyen, A. Cassell, J. Han and M. Meyyappan, *Science,* 2003, **300**, 1249-1249.

(22) B. Cheng, J. M. Russell, W. Shi, L. Zhang and E. T. Samulski, *J. Am. Chem. Soc.,* 2004, **126**, 5972-5973.

(23) K. Suito, N. Kawai and Y. Masuda, *Mater. Res. Bull.,* 1975, **10**, 677-680.

(24) L. G. Liu, *Science,* 1978, **199**, 422-425.

(25) C. H. Shek, J. K. L. Lai, G. M. Lin, Y. F. Zheng and W. H. Liu, *J. Phys. Chem. Solids,* 1997, **58**, 13-17.

(26) L. Kaplan, A. Ben-Shalom, R. L. Boxman, S. Goldsmith, U. Rosenberg and M. Nathan, *Thin Solid Films,* 1994, **253**, 1-8.

(27) L.Y. Kong, J. Ma, Z. Zhu, C. Luan, X. H. Yu and Q. Q. Yu, *Mater. Lett.,* 2010, **64**, 1350-1353.

(28) Z. W. Chen, J. K. L. Lai and C. H. Shek, *Appl. Phys. Lett.,* 2006, **89**, 231902-231904.

(29) Z. W. Chen, M. H. Wu, C. H. Shek, C. M. L. Wu and J. K. L. Lai, *Chem. Commun.*, 2015, **51**,

1175-1184.

(30) Z. M. Tian, S. L. Yuan, J. H. He, P. Li, S. Q. Zhang, C. H. Wang, Y. Q. Wang, S. Y. Yin and L. Liu, *J. Alloys Compd.,* 2008, **466**, 26-30.

(31) L. Sangaletti, L. E. Depero, A. Dieguez, G. Marca, J. R. Morante, A. Romano-Rodriguez and G. Sberveglieri, *Sens. Actuat. B*, 1997, **44**, 268-274.

(32) J. Haines and J. M. Léger, *Phys. Rev. B*, 1997, **55**, 11144-11154.

(33) V. E. Müller, *Acta Crystallogr. B*, 1984, **40**, 359-363.

(34) J. Arbiol, E. Comini, G. Faglia, G. Sberveglieri and J. R. Morante, *J. Cryst. Growth*, 2008, **310**, 253-260.

(35) N. H. Hong, J. Sakai, W. Prellier and A. Hassini, *J. Phys.: Condens. Matter.*, 2005, **17**, 1697-1702.

(36) B. Sathyaseelan, K. Senthilnathan, T. Alagesan, R. Jayavel and K. Sivakumar, *Mater. Chem. Phys.,* 2010, **124**, 1046-1050.